Electronic Supplementary Information (ESI)

Spectroscopic characterization of the key catalytic intermediate Ni-C in the O_2-tolerant [NiFe] Hydrogenase I from *Aquifex aeolicus*: evidence of a weakly bound hydride

Maria-Eirini Pandelia[a], Pascale Infossi[b], Matthias Stein[c], Marie-Thérèse Giudici-Orticoni[b], and Wolfgang Lubitz*[a]

[a]*Max-Planck-Institut für Bioanorganische Chemie, Stiftstrasse 34-36, 45470, Mülheim a.d. Ruhr, Germany. E-mail: wolfgang.lubitz@mpi-mail.mpg.de*
[b]*Laboratoire de Bioénergétique et Ingénierie des Protéines, IMM-CNRS, 13402, Marseille, France. E-mail : giudici@ifr88.cnrs-mrs.fr*
[c]*Max-Planck-Institut für Dynamik komplexer technischer Systeme, Sandtorstrasse 1,39106 Magdeburg, Germany. E-mail: matthias.stein@mpi-magdeburg.mpg.de*

Materials and Methods

Sample purification and preparation. The Hase I-cyt*b* complex from *Aquifex aeolicus* was purified as previously described[1]. Reduction with H_2 (N27, Air Liquide) and $^2H_2$ (Air Liquide) was performed in tri-distilled H_2O and highly enriched ^2H_2O (99, 9 %, Deutero GmbH) Tris- (pH 7.4, pD = 7.4) and MES- (pH 6.4, pD = 6.4) based buffers, respectively. The reduction was carried out in the X- or Q-band tubes using a homebuilt gas line.

For the Mims ENDOR measurements samples of approximately 250μM were used. The Ni-C state could be maximized in the samples after reduction with $H_2/^2H_2$ for 50-60 min. The longer times were used for the deuterated samples. The Ni-C signal is weak, since Ni-C represents an intermediate state of the catalytic cycle (only 0.2-0.4 spins/mol) and could be maximized in buffer solutions of lower pH (6.4)[2]. In particular, in the [NiFe] hydrogenase from *A. aeolicus*, Ni-C has been observed to be a more transient species and thus a more difficult intermediate to trap. Samples of higher concentration (~400 μM) were used for the HYSCORE experiments and for recording the EPR spectra. However, it was not possible to record any meaningful ENDOR spectra, due to an enhancement of the spin-spin relaxation time (T_2). The increased sample concentration enhanced processes that cause loss of the magnetization in the *x*-*y* plane and thus did not lead to any improvement of the signal-to-noise **ratio in the ENDOR measurements. 25 % of deuterated glycerol (Sigma-**Aldrich) was added to the sample, so as to increase the T_2 relaxation times, but no improvement could be observed.

Magnetic coupling with the reduced proximal iron-sulfur center offers an additional complication; fortunately this exchange interaction is only one half of that observed in standard hydrogenases (Figure S1). The excitation bandwidth of the non-selective microwave pulses used for the Mims ENDOR measurements is larger than the splitting caused by the exchange-interaction between [NiFe] and the reduced proximal [4Fe] cluster. The orientation selectivity in our EPR spectra caused by the exchange interaction has been accounted for by increasing the excitation bandwith used in the simulations. In HYSCORE spectra, signals from ^{14}N nuclei complicate the analysis due to overlap with the ^2H signals[3].

Fourier Transform Infrared spectroscopy: Infrared measurements were performed on a Bruker IFS 66v/s FTIR spectrometer with 2 cm^{-1} resolution. The detector was a photovoltaic mercury cadmium telluride (MCT) element. Time resolved measurements at cryogenic temperatures were carried out in an Optistat CF cryostat with an ITC 503 temperature

controller (Oxford Instruments). *In-situ* illumination for 5 minutes was performed with a slide projector (250 W halogen lamp, 24 V) equipped with an electronic shutter (Compor). The low temperature FTIR cell consists of two sapphire windows with optical path-length of 80 µm. The software for data recording consisted of the OPUS package (Bruker Optics). Analysis and further processing was performed with home-built routines written in MATLAB 6.5 (Mathworks).

Continuous wave (CW) EPR: CW EPR measurements were carried out at a Bruker ESP300 CW X-Band spectrometer (operating at approx. 9.4 GHz) using a rectangular cavity (TE_{102}) and a continuous helium flow cryostat (Oxford 910) with a temperature controller (Oxford ITC 503). The first-derivative EPR spectra were simulated using the MATLAB (Mathworks) based *EasySpin* simulation software by taking into account *A*- and *g*-strain effects contributing to the inhomogeneous linewidth of the EPR lines.

Pulse EPR: Pulsed EPR measurements were carried out at X-band (~9.7 GHz) frequencies in a Bruker Elexsys E-580 FT EPR X-band spectrometer equipped with a dielectric resonator at cryogenic temperatures using a helium flow cryostat (Oxford Instruments). Pulsed EPR measurements at Q-Band (~34.0 GHz) were carried out on a Bruker Elexsys E-580 FT EPR Q-band spectrometer with a homebuilt ENDOR resonator[4]. The solid-state microwave amplifier in this bridge produces a power of 2 W at the resonator, which is sufficient for obtaining a MW π/2 pulse of 16 ns. Cryogenic temperatures (7−10 K) were reached using an Oxford CF935 flow cryostat. A low-pass filter (Trilithic) was used to cut off the ^{1}H harmonics. A high-power RF amplifier (2.5 kW, Amplifier Research 2500L, 10 kHz-220 MHz) was used to achieve short radiofrequency pulses (8 µs for ^{1}H and 33 µs for ^{2}H).
EPR spectra were obtained by integration over the two-pulse echo sequence (π/2-τ-π/2). Typical π/2 lengths were 8 ns (X-Band) and 16-36 ns (Q-band). Pulse Electron Nuclear DOuble Resonance (ENDOR) spectra of *A. aeolicus* [NiFe] hydrogenase (in H_2O and $^{2}H_2O$) were recorded using the Mims ENDOR sequence (π/2-τ- π/2- π_{RF}-t- π/2). The ENDOR efficiency is described by[5]:

$$F_{ENDOR} = \frac{1}{4}\left(1 - \cos(A_{eff} \cdot \tau)\right) \qquad \text{(Eq. 1)}$$

Due to the blind-spot behaviour (τ dependence) of the Mims sequence the optimum separation of the first two π/2 pulses was chosen to be 320 ns (the first blind-spot is ± 1.56 MHz centred

on the ^{2}H Larmor frequency). The total intensity of the stimulated echo of the Mims sequence scales with $\exp(-\frac{\tau}{T_2})$.

Hyperfine sublevel correlation spectroscopy experiments (HYSCORE, $\pi/2$-τ-$\pi/2$-t_1-π-t_2- $\pi/2$) were measured at the principal orientations of the *g*-tensor of the Ni-C state for several τ values (τ = 124 ns was chosen for X-Band, and τ = 328 ns for Q-Band). The absorption EPR spectra were simulated using the MATLAB (Mathworks) based *EasySpin*[6] simulation software by taking into account *A*- and *g*-strain effects contributing to the inhomogeneous linewidth of the EPR lines. The full spin Hamiltonian for an exchange-coupled two-spin system can be written as[7] :

$$H = -2J\vec{S}_1\vec{S}_2 + \vec{S}_1\mathbf{d_{12}}\vec{S}_2 + \sum_{i=1,2}\mu_B\vec{B}_0\mathbf{g_i}\vec{S}_i \qquad \text{(Eq. 2)},$$

where the first term is the Heisenberg exchange. In this article, we consider only the isotropic part of the exchange coupling tensor *J*, because the anisotropic part is typically small and it is complicated to evaluate from EPR data. The second term in Eq. 2 is the magnetic dipolar coupling. Dipolar coupling mainly depends on the distance between paramagnetic centers. Using the point-dipole approximation the tensor $\mathbf{d}_{12}$ can be expressed as:

$$\mathbf{d_{12}} = \frac{\mu_B^2}{r^3}\left(\mathbf{g_1 g_2} - \frac{3(\mathbf{g}_1\vec{r})(\mathbf{g}_2\vec{r})}{r^2}\right) \qquad \text{(Eq. 3)},$$

where *r* is the distance vector between the two paramagnetic centers and g_1 and g_2 are the g-factors of the two centers (considered to be anisotropic). A more accurate description of the magnetic interaction between the [NiFe] site and the reduced proximal [4Fe] cluster would require exact knowledge of the projection factors of the dipolar interaction between each Fe ion of the cluster and the [NiFe] site. The last term of Eq. 2 contains the electronic Zeeman interaction.

Table S1: Principal *g*-values of the Ni-C state and its light-induced photoproduct states in the Hase I from *Aquifex aeolicus* (this work), in the regulatory hydrogenase (RH) from *Ralstonia eutropha*[8] and the periplasmic hydrogenase from *Desulfovibrio vulgaris* Miyazaki F[9].

	A. aeolicus **(Hase I)**		***R. eutropha*** **(RH)**		***D. vulgaris* MF** **(periplasmic)**	
	g_i		g_i		g_i	
	Ni-C	**Ni-L1** **Ni-L2**	**Ni-C**	**Ni-L1** **Ni-L2**	**Ni-C**	**Ni-L2**
x	2.211	2.334 2.281	2.197	2.251 2.305	2.198	2.298
y	2.149	2.152 2.121	2.139	2.094 2.077	2.142	2.116
z	2.013	2.049 2.050	2.015	2.046 2.054	2.012	2.045

Table S2: IR stretching vibrations of the CO and CN^- ligands of the Fe ion as measured for the Ni-C state of Hase I from *A. aeolicus* and its light-induced photoproducts at various temperatures.

	$\bar{\nu}_{CO}$, **cm^{-1}**	$\bar{\nu}_{CN\ (asym)}$, **cm^{-1}**	$\bar{\nu}_{CN\ (sym)}$, **cm^{-1}**
Ni-C (100 K)	1952	2080	2092
Ni-L2 (100 K)	1901	2049	2068
Ni-C (200 K)	1950	2078	2091
Ni-L1 (200 K)	1862	2025	2045
Ni-L3 (130 K)	1872	2033	2056

Figure S1: CW EPR spectrum of the Ni-C state recorded in the dark. At these low temperatures the Ni-L1 state is also present in the spectra even in the absence of illumination (refer to Table S1). In these spectra, the magnetic interaction of the proximal [4Fe] cluster with the paramagnetic [NiFe] site manifests itself mainly in the splitting of the Ni-C and Ni-L2 signals. The simulation of the EPR spectra (here depicted in grey colour) showed that the isotropic magnetic interaction between the [NiFe] site in the Ni-C state (S = 1/2) and the reduced proximal [4Fe] cluster (S = 1/2) is $2J = 38(\pm2)\cdot10^{-4}$ cm^{-1} = 114 MHz and between the Ni-L1 state (S = 1/2) and the proximal [4Fe] cluster is $2J = 36(\pm2)\cdot10^{-4}$ cm^{-1} = 108 MHz. Thus, the magnitude of the magnetic interaction observed in the case of the Ni-C state of *A. aeolicus* Hase I is only half of that reported for the Ni-C state in the *Desulfovibrio gigas* hydrogenase[10]. Experimental Conditions: T = 10 K, MW Freq = 9.455 GHz, modulation amplitude = 1 mT, MW Power = 1.997 mW.

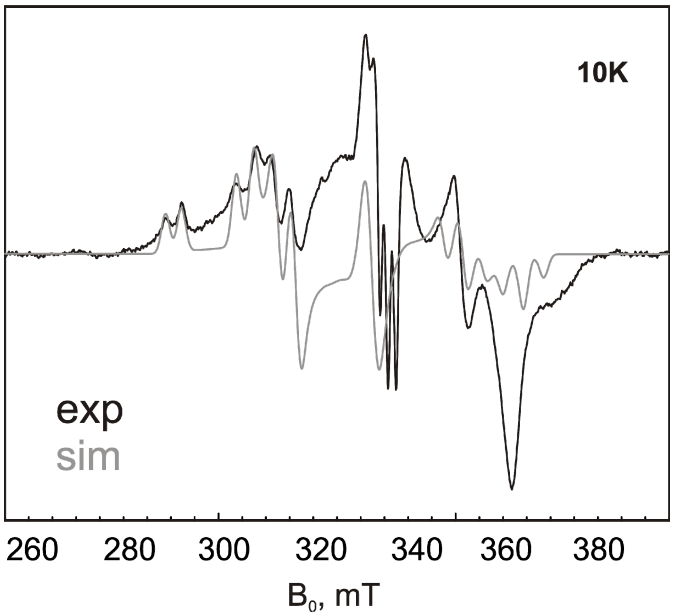

Figure S2: 2-pulse echo-detected EPR absorption spectrum of the Ni-C state recorded at Q-band. The spectrum has been simulated using the isotropic exchange obtained by the spectrum in Fig. S1. The spectrum of the distal [4Fe4S] cluster (g_z =2.033, g_y = 1.910, g_x= 1.862)[11], which is also reduced (S = 1/2), has also been simulated. Experimental Conditions: T = 7 K, MW Freq. = 34.10 GHz, $\pi/2$ = 16 ns, τ = 320 ns, Shot Repetition Time (SRT) 4 ms. Asterisks denote overlapping contributions from Mn^{2+} impurities. The low-field features in the spectrum originate from background contributions and residual signals of Ni-L1 already present in the dark.

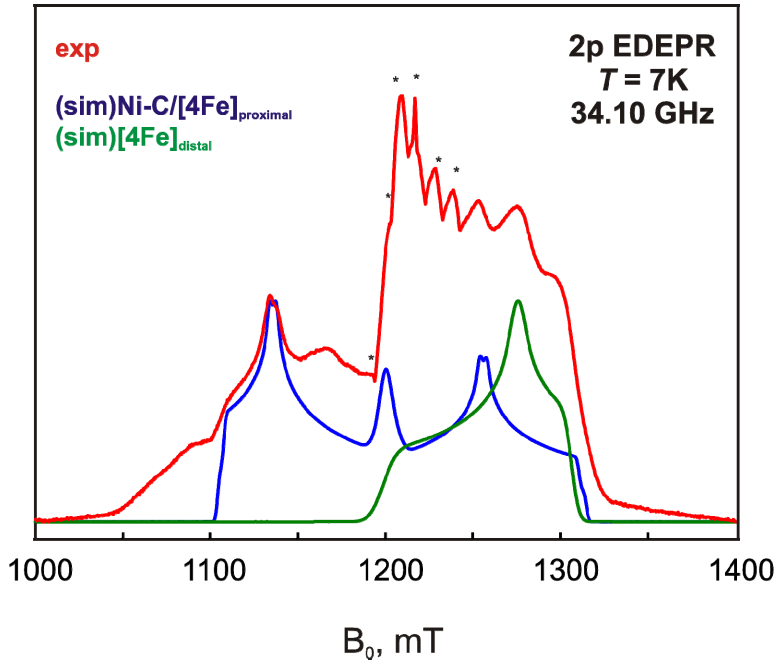

Table S3: Effective ^{2}H hyperfine interaction parameters obtained for the H/^{2}H exchangeable hydride bridge of the Ni-C state of the [NiFe] Hydrogenase I from *A. aeolicus*. The directions of the hyperfine tensor are given with reference to the *g*-tensor frame (g_x, g_y, g_z) that was determined earlier for the *D. vulgaris* MF hydrogenase[12]. The error in the determination of the magnitude of the hyperfine tensor components is ± 0.15 MHz. The signal-to-noise ratio of the ENDOR data, as well as the resolution of our HYSCORE data precludes a definitive assignment of the direction of the exchangeable proton (H-bridge) hyperfine tensor. We are limited by the quality of the data to only propose a generic solution. The orientation of the tensor proposed according to the present data, is somewhat different from that published earlier on the systems of *D. vulgaris* MF and *R. eutropha* (RH), but the main component still lies along the g_x direction[8]. The magnitude of the quadrupole interaction is small, but has been taken into account.

	A_x, MHz	**A_y, MHz**	**A_z, MHz**	**Aiso**	**$\lvert (e^2qQ/h) \rvert$, kHz**
A. aeolicus	1.95	-0.95	-1.80	-0.27	160
D. vulgaris MF	2.82	-2.76	-1.67	-0.57	-
R. eutropha (RH)	2.82	-2.76	-1.67	-0.57	200

Table S4: The ^{14}N hyperfine and quadrupole values of the N_ε nitrogen of the histidine that is hydrogen bonded to the apical thiol ligand have been obtained from HYSCORE measurements on the Ni-C samples and are given in the table below. For comparison the hyperfine and quadrupole parameters obtained for the periplasmic hydrogenase from *D. vulgaris* MF[3,9], *D. gigas*[13], *T. roseopersicina* (HynSL)[14] and the membrane-bound hydrogenase from *R. eutropha*[15] have been included for comparison. When the effective hyperfine coupling A of a ^{14}N nucleus equals twice the nuclear Zeeman frequency ν_n, the condition of the so-called exact-cancellation is fulfilled; the hyperfine and nuclear Zeeman interactions cancel out in one m_s manifold and the 'pure' quadrupole frequencies (ν_0, ν_- , ν_+) are observed. From these frequencies the quadrupole parameter $K = (e^2qQ)/4h$ and the asymmetry parameter η can be determined; $\nu_\pm = K(3 \pm \eta)$ and $\nu_0 = 2K\eta$. Based on the ESEEM measurements we obtain ν_0 = 0.40 MHz, ν_+ = 1.67 MHz, ν_-= 1.22 MHz. The nuclear quadrupole interaction parameters, i.e. the quadrupole coupling constant $\boldsymbol{(e^2qQ/h)}$ and the asymmetry parameter $\boldsymbol{\eta}$ measure the magnitude and the symmetry of the electric-field gradient tensor. The effective isotropic hyperfine interaction of the ^{14}N imidazole nitrogen N_ε in the case of the *A. aeolicus* Hase I is A_{iso} = 1.54 MHz.

	A_x, MHz	A_y, MHz	A_z, MHz	$\lvert (e^2qQ/h)\rvert$, MHz[a]	η
A. aeolicus (Ni-C)	+1.33	+1.22	+2.07	1.92	0.40
D. vulgaris MF					
(Ni-B)	+1.32	+1.32	+2.07	1.90	0.37
(Ni-C)	+1.50	+1.50	+2.70	1.88	0.39
D. gigas (Ni-C)				1.90	0.40
R. eutropha (Ni-B)				1.94	0.38
T. roseopersicina (Ni-A)				1.93	0.38

[a] The sign of the quadrupole interaction has been assigned to be negative based on theoretical calculations of the electric field gradient tensor[16] and based on DFT calculations in the work by Agrawal et al[3].

Figure S3: Control Mims ENDOR experiments performed on fully protonated samples of the Ni-C state. Experimental Conditions: $\pi/2$ = 36 ns, τ = 320 ns, π_{RF} = 33 µs, T = 7 K. Each spectrum has been averaged for 48 hours. Note that there are no ^{2}H ENDOR signals present (compare with Fig. 4 in the main manuscript).

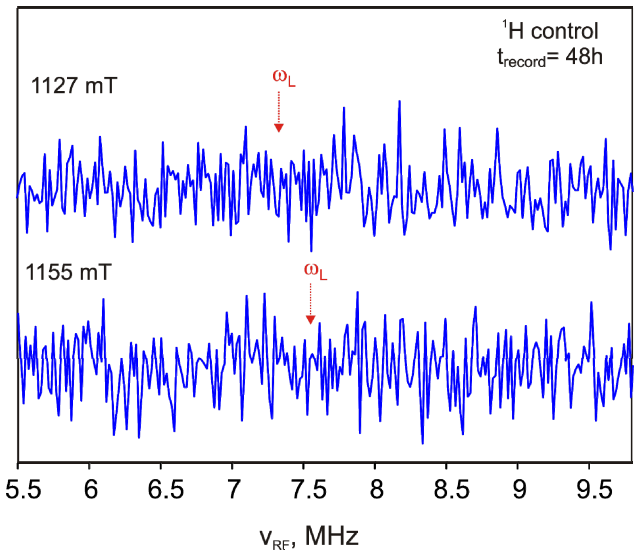

DFT calculations

Structural optimizations were started from the high resolution protein crystal structure of the reduced form of [NiFe] hydrogenase from *D. vulgaris* MF[17]. Cysteine amino acid residues were truncated after the C_β atoms and saturated with hydrogens. All calculations were performed using Orca v.2.8.0 [18].

Geometry optimizations were performed using the BP86 exchange-correlation functional[19,20] and a double-zeta basis set[21] with polarization functions that were obtained from the TURBOMOLE library (ftp://ftp.chemie.uni-karlsruhe.de/pub/basen). In addition, single-point calculations using the hybrid B3LYP functional[22,23,24,25] at the BP86/TZVP geometry optimized structures were carried out. IR spectra were generated by numerically calculating the second derivatives. Calculations of g-tensors were performed using an effective mean-field spin-orbit coupling operator and the center-of-mass as the origin of the *g*-tensor[26,27,28].

Fully relaxed structural optimizations led to structural parameters in good agreement with the X-ray structure: Ni···Fe distance 2.58 Å, Ni···H- distance 1.59 Å, Fe···H distance 1.71 Å and angle <(Ni···H···Fe) 102.6º.

For modeling the hydride binding situation in *A. aeolicus*, structural optimization of only the hydrogen atoms was performed. The position of the heavy atoms can be determined with sufficient accuracy at the resolution of 1.50 Å, but the positioning of the μ-hydride in Ni-C and the protons of the cysteine amino acid residues is not known. The Ni-C bonding situation was scanned by varying the Ni-H^- bond distances from 1.62 Å to 3.42 Å in increments of 0.1 Å. EPR g-values were calculated with the B3LYP functional which was shown to give superior results to pure exchange-correlation functionals for g-tensor principal values. ^{1}H hyperfine coupling parameters were calculated using the BP86 exchange-correlation functional, which was shown to give good results for transition metal complexes and [NiFe] active site models[29].

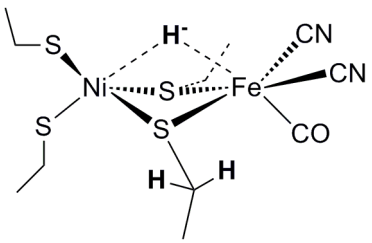

Table S5: Calculated *g*-tensor principal values and ^{1}H hyperfine coupling constants for various hydride binding situations

For the β-CH_2 protons, the influence of spin-orbit coupling on the hyperfine tensor was found to be very small of the order of -0.16 for A_x to +0.16 for A_z MHz leading to an isotropic pseudo-contact interaction of -0.02 MHz.

For the bridging hydride between the two transition metal ions, the second-order contribution from spin-orbit coupling was found to be of larger magnitude and the full hyperfine tensor containing spin-orbit coupling and the inclusion of pseudo-contact interaction in the isotropic hyperfine coupling constant are given in red.

Distance /Å		Angle /degrees	*g*-Tensor Principal Values B3LYP/DZP	^{1}H-hfc [MHz] BP86/DZP	
Ni···H$^-$	Fe···H$^-$	<(NiH$^-$Fe)	g_x, g_y, g_z	β-C$\underline{H_2}$-Cys (A_{tot}), a_{iso}	Ni-μ$\underline{^{1}H}$-Fe (A_{tot}), a_{iso}
1.62	1.72	100.7	2.20, 2.15, 2.03	(+16, +18, +22) +19 (+10, +10, +15) +12	(-9.9, +10.6, -15.0) -4.8 (-10.0, +13.0, -16.0) -4.3
1.72	1.70	97.4	2.21, 2.16, 2.03	(+16, +18, +22) +19 (+10, +10, +15) +12	(-7.4, +9.5, -12.4) -3.4 (-7.6, +11.7, -13.2) -3.0
1.82	1.69	94.1	2.21, 2.17, 2.04	(+16, +18, +22) +18 (+10, +10, +15) +12	(-5.4, +8.8, -10.2) -2.3 (-5.6, +10.6, -10.9) -2.0
1.92	1.69	90.7	2.21, 2.18, 2.05	(+16, +17, +22) +18 (+10, +10, +15) +12	(-3.8, -8.3, +8.4) -1.2 (-4.0, -9.0. +10.0) -1.0
2.02	1.69	87.3	2.21, 2.18, 2.05	(+15, +17, +21) +18 (+10, +10, +14) +12	(-2.7, -6.8, +8.1) -0.5 (-2.8, -7.3, +9.4) -0.2
2.12	1.70	83.9	2.22, 2.19, 2.05	(+15, +17, +21) +18 (+10, +10, +14) +12	(-1.5, -5.3, +8.0) +0.4 (-1.7, -5.8, +9.2) +0.6
2.22	1.71	80.6	2.23, 2.20, 2.06	(+15, +16, +21) +18 (+10, +10, +14) +11	(-0.4, -3.8, +8.3) +1.3 (-0.6, -4.2, +9.3) +1.5
2.32	1.73	77.3	2.24, 2.21, 2.07	(+15, +17, +21) +17 (+10, +10, +14) +11	(-0.2, -3.2, +8.0) +1.6 (-0.3, -3.4, +8.9) +1.7
2.42	1.76	74.1	2.24, 2.21, 2.06	(+14, +16, +20) +17 (+10, +10, +14) +11	(+0.4, -2.1, +7.9) +2.0 (+0.3, -2.4, +8.8) +2.2
2.52	1.79	71.0	2.26, 2.22, 2.08	(+14, +16, +20) +17 (+10, +10, +14) +11	(+1.2, -1.0, +8.3) +2.8 (+1.1, -1.3, +9.0) +2.9
2.62	1.82	68.1	2.25, 2.22, 2.06	(+14, +16, +20) +17 (+9, +10, +14) +11	(+0.1, +2.0, +8.6) +3.5 (-0.3, +1.9, +9.2) +3.6
2.72	1.86	65.2	2.25, 2.22, 2.06	(+14, +16, +20) +16 (+9, +10, +14) +11	(+2.5, +2.5, +10.4) +5.7 (+2.3, +4.2, +11.0) +5.8
2.82	1.91	62.5	2.25, 2.22, 2.06	(+13, +15, +19) +16 (+9, +10, +14) +11	(+2.0, +3.4, +9.3) +4.9 (+1.8, +3.3, +9.8) +5.0
2.92	1.95	59.9	2.25, 2.18, 2.04	(+14, +15, +19) +16 (+9, +10, +14) +11	(+3.9, +5.1, +10.6) +6.5 (+3.7, +5.0, +11.0) +6.6
3.02	2.01	57.4	2.25, 2.20, 2.04	(+13, +15, +19) +16	(+6.1, +7.1, +12.2) +8.5

				(+9, +10, +13) +11	(+5.9, +7.0, +12.7) +8.5
3.12	2.06	55.1	2.24, 2.16, 2.01	(+13, +15, +19) +16 (+9, +10, +13) +11	(+10.2, +11.0, +15.9) +11 (+10.0, +11.0, +16.3) +12.4
3.22	2.12	52.9	2.24, 2.14, 2.01	(+13, +14, +19) +15 (+9, +10, +13) +11	(+14.9, +15.7, +20.2) +17.0 (+14.8, +15.6, +20.6) +17.0
3.32	2.18	50.8	2.24, 2.13, 2.00	(+13, +14, +18) +15 (+9, +10, +13) +11	(+32.5, +33.1, +37.8) +34.4 (+32.5, +33.2, +37.4) +34.4
3.42	2.25	48.8	2.23, 2.09, 1.97	(+13, +14, +18) +15 (+9, +10, +13) +11	(+66.3, +67.0, +71.0) +68.1 (+66.2, +66.9, +71.3) +68.2

At a Ni···H distance of 1.82 Å, one obtains *g*-tensor principal values of (g_x, g_y, g_z = 2.21, 2.17, 2.04) which show an upshift of the g_x, g_y components compared to the binding situation in standard hydrogenases (g_x, g_y, g_z = 2.20, 2.15, 2.03)[12,9].

Figure S6: Calculated g-tensor orientation for Ni-C in *A. aeolicus* with a Ni···H distance of 1.82 Å. The g-tensor orientation is very similar to that of the Ni-C state in *D. vulgaris* MF. The Ni-H bond points towards the direction of the g_x axis.

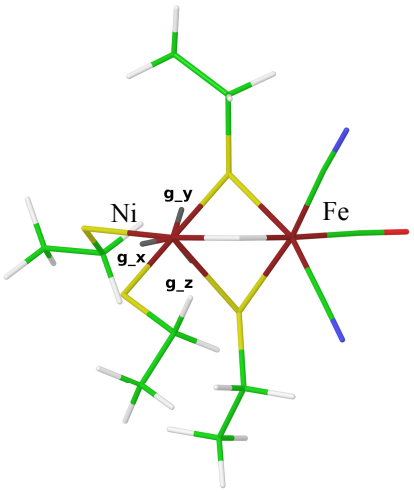

The β-cysteinyl protons are rather insensitive to a variation of the hydride binding position, whereas the isotropic and dipolar ^{1}H hyperfine coupling constants of the bridging hydride show a strong dependence on the Ni···H bond distance.

At a Ni···H distance of 1.82 Å, the isotropic hyperfine coupling constant is -2.3 MHz and the dipolar hyperfine tensor A'_{dip} = (-3.6, +12.6, -8.9) MHz (considering second-order effects

from spin-orbit coupling); this is in very good agreement with the experimentally determined one in the present work for Hase I (a_{iso} = -1.76 MHz, A'_{dip} (-4.4, +14.5, -10) MHz. From the simulations of the EPR/ENDOR spectra the largest positive dipolar component of the A-tensor lies rather along the g_y than along the g_x direction. This is different from the situation predicted by the DFT calculations and previous measurements on standard hydrogenases[9,12]. This difference remains to be elucidated; it should be considered that the uncertainty in the A-tensor direction determination is large in the present study making a unique assignment of the orientation very difficult.

References and Notes

1. M. Brugna-Guiral, P. Tron, W. Nitschke, K. O. Stetter, B. Burlat, B. Guigliarelli, M. Bruschi and M. T. Giudici-Orticoni, *Extremophiles*, 2003, **7**, 145-157.

2. M. E. Pandelia, V. Fourmond, P. Tron-Infossi, E. Lojou, P. Bertrand, C. Léger, M. T. Giudici-Orticoni and W. Lubitz, *J. Am. Chem. Soc.*, 2010, **132**, 6991-7004.

3. A. G. Agrawal, M. van Gastel, W. Gärtner and W. Lubitz, *J. Phys. Chem. B*, 2006, **110**, 8142-8150.

4. E. Reijerse, F. Lendzian, R. Isaacson, W. Lubitz, *J. Magn. Res.,* in press, DOI:10.1016/j.jmr.2011.11.011

5. C. Gemperle and A. Schweiger, *Chem. Rev.*, 1991, **91**, 1481-1505.

6. S. Stoll and A. Schweiger, *J. Magn. Res.*, 2006, **178**, 42-55.

7. A. Bencini and D. Gatteschi, *Electron Paramagnetic Resonance of Exchange Coupled Systems. Springer-Verlag New York, Inc.: Secaucus, New Jersey, USA; Berlin, West Germany. Illus*, 1990

8. M. Brecht, M. van Gastel, T. Buhrke, B. Friedrich and W. Lubitz, *J. Am. Chem. Soc.*, 2003, **125**, 13075-13083.

9. S. Foerster, M. van Gastel, M. Brecht and W. Lubitz, *J. Biol. Inorg. Chem.*, 2005, **10**, 51-62.

10. B. Guigliarelli, C. More, A. Fournel, M. Asso, E. C. Hatchikian, R. Williams, R. Cammack and P. Bertrand, *Biochemistry*, 1995, **34**, 4781-4790.

11. M. E. Pandelia, W. Nitschke, P. Infossi, M. T. Giudici-Orticoni, E. Bill and W. Lubitz, *Proc. Natl. Acad. Sci. USA*, 2011, **108**, 6097-6102.

12. S. Foerster, M. Stein, M. Brecht, H. Ogata, Y. Higuchi and W. Lubitz, *J. Am. Chem. Soc.*, 2003, **125**, 83-93.

13. A. Chapman, R. Cammack, C. E. Hatchikian, J. McCracken and J. Peisach, *FEBS Lett.*, 1988, **242**, 134-138.

14. R. Cammack, K. L. Kovacs, J. McCracken and J. Peisach, *Eur. J. Biochem.*, 1989, **182**, 363-366.

15. M. Saggu, C. Teutloff, M. Ludwig, M. Brecht, M. E. Pandelia, O. Lenz, B. Friedrich, W. Lubitz, P. Hildebrandt, F. Lendzian and R. Bittl, *Phys. Chem. Chem. Phys.*, 2010, **12**, 2139-2148.

16. M. H. Palmer, F. E. Scott and J. A. S. Smith, *Chem. Phys.*, 1983, **74**, 9-14.

17. H. Ogata, S. Hirota, A. Nakahara, H. Komori, N. Shibata, T. Kato, K. Kano and Y. Higuchi, *Structure*, 2005, **13**, 1635-1642.

18. F. Neese, T. Petrenko, D. Ganyushin and G. Olbrich, *Coord. Chem. Rev.*, 2007, **251**, 288-327.

19. A. D. Becke, *Phys.Rev. A*, 1988, **38**, 3098-3100.

20. J. P. Perdew, *Phys.Rev. B*, 1986, **33**, 8822-8824.

21. A. Schäfer, H. Horn and R. Ahlrichs, *J. Chem. Phys.*, 1992, **97**, 2571-2577.

22. A. D. Becke, *J. Chem. Phys.*, 1993, **98**, 1372-1377.

23. C. T. Lee, W. T. Yang and R. G. Parr, *Phys.Rev. B*, 1988, **37**, 785-789.

24. S. H. Vosko, L. Wilk and M. Nusair, *Canad. J.Phys.*, 1980, **58**, 1200-1211.

25. P. J. Stephens, F. J. Devlin, C. F. Chabalowski and M. J. Frisch, *J. Phys. Chem.*, 1994, **98**, 11623-11627.

26. F. Neese, *J. Chem. Phys.*, 2005, **122**,

27. F. Neese, *J. Chem. Phys.*, 2001, **115**, 11080-11096.

28. F. Neese, *Int. J. Quant. Chem.*, 2001, **83**, 104-114.

29. M. Stein, 2001, Doctoral Dissertation, Technical University Berlin